FeSi diffusion barriers in Fe/FeSi/Si/FeSi/Fe multilayers and oscillatory antiferromagnetic exchange coupling



2008 J. Phys.: Condens. Matter 20 425205

(http://iopscience.iop.org/0953-8984/20/42/425205)

J. Phys.: Condens. Matter **20** (2008) 425205 (8pp) doi:10.1088/0953-8984/20/42/425205

# FeSi diffusion barriers in Fe/FeSi/Si/FeSi/Fe multilayers and oscillatory antiferromagnetic exchange coupling

**F Stromberg[1], S Bedanta[1], C Antoniak[1], W Keune[1,2] and H Wende[3]**

[1] Fachbereich Physik, Universität Duisburg-Essen (Campus Duisburg), D-47048 Duisburg, Germany
[2] Max-Planck-Institut für Mikrostrukturphysik, D-06120 Halle, Germany
[3] Fachbereich Physik and Center for Nanointegration (CeNIDE), Universität Duisburg-Essen (Campus Duisburg), D-47048 Duisburg, Germany

E-mail: fstromberg@gmx.de

Received 11 July 2008, in final form 21 August 2008
Published 16 September 2008
Online at stacks.iop.org/JPhysCM/20/425205

**Abstract**

We study the diffusion of $^{57}$Fe probe atoms in Fe/FeSi/Si/FeSi/Fe multilayers on Si(111) prepared by molecular beam epitaxy by means of $^{57}$Fe conversion electron Mössbauer spectroscopy (CEMS). We demonstrate that the application of FeSi boundary layers successfully inhibits the diffusion of $^{57}$Fe into the Si layer. The critical thickness for the complete prevention of Fe diffusion takes place at a nominal FeSi thickness of $t_{\mathrm{FeSi}} = 10$–$12$ Å, which was confirmed by the evolution of the isomer shift $\delta$ of the crucial CEM subspectrum. The formation of the slightly defective c-FeSi phase for thicker FeSi boundary layers (∼20 Å) was confirmed by CEMS and reflection high-energy electron diffraction (RHEED). Ferromagnetic resonance (FMR) shows that, for $t_{\mathrm{FeSi}} = 0$–$14$ Å, the Fe layers in all samples are antiferromagnetically coupled and we observe an oscillatory antiferromagnetic coupling strength with FMR and superconducting quantum interference device (SQUID) magnetometry for varying FeSi thickness with a period of ∼6 Å.

(Some figures in this article are in colour only in the electronic version)

## 1. Introduction

Due to the strong antiferromagnetic (AF) exchange coupling (EC) between the Fe layers in Fe/Si/Fe layered structures, which can be even stronger than in purely metallic multilayers [1], there has been increasing interest in these systems during the last few years [2–4]. However, the underlying mechanism for this unusual EC still remains elusive. The experimental complications arise from the high reactivity of the Fe/Si interface, even at room temperature (RT).

Many studies on the phase formation upon depositing Fe on Si substrates were conducted in the last few years. Depending on the thickness of the Fe layer, different phases (stable and metastable) are formed [5–9]. The common observations are the formation of a disordered structure for low Fe coverages (about 3 monolayers (ML) Fe), which has a composition close to FeSi. Upon further evaporation of Fe an amorphous magnetic phase similar to $Fe_3Si$ evolves (starting from about 8 ML Fe). For about 20 ML or more Fe coverage one obtains a structure consisting of the disordered FeSi interface, $\alpha$-Fe(Si) and pure $\alpha$-Fe. Upon annealing at intermediate temperatures the metastable c-FeSi phase forms, and after annealing at higher temperatures $\epsilon$-FeSi and $\beta$-$FeSi_2$ emerge. The direct observation of the metastable c-$Fe_{1-x}Si$ phase at the Fe/Si interfaces was a major issue in the notion that this phase is responsible for mediating the EC across the Si layer in Fe/Si/Fe sandwiches or multilayers [10]. This was based on band structure calculations by Moroni *et al* [11]. Their result showed a peak of the density of states 0.2 eV above the Fermi level for both stoichiometric

 

c-FeSi and defective c-$Fe_{1-x}Si$. The EC was thought to be generated by sd-mixing within the Anderson model. On the other hand, Imazono *et al* [12] applied SXF (soft x-ray fluorescence spectroscopy) to detect the $Fe_{1-x}Si_x$ composition in sputtered Fe/Si multilayers and proposed a model implying the formation of amorphous $FeSi_2$ and $Fe_3Si$ in the nominally 13 Å thick amorphous Si interlayers. The EC was found to be antiferromagnetic (AF) for this Si thickness (and also for 10 and 15 Å a-Si). Most interestingly, Endo *et al* [13] showed that initially non-coupled Fe/Si/Fe multilayers with a thick a-Si layer convert to an AF coupled state after annealing. The main conclusion was that the EC is mediated by crystalline silicides in the interlayer. Later, these researchers successfully applied the quantum interference model [14] to describe the temperature dependence of the bilinear and biquadratic coupling constants for samples with different Si content, ranging from insulating to metallic behavior [15]. A very strong EC for nominally pure Si interlayers and a simultaneous exclusion of the formation of metallic c-FeSi at the interfaces was found by Bürgler *et al* [16]. They observed various phases (from $Fe_3Si$ to semiconducting $FeSi_2$)with soft x-ray emission (SXE) and near-edge x-ray absorption spectroscopy (NEXAFS). Resistivity measurements perpendicular to the film plane showed a nonlinear $I$–$V$ characteristic which was assigned to an insulating or semiconducting material in the spacer region. Using wedge-type samples Bürgler *et al* could also measure the dependence of the EC for different interlayer thicknesses and compositions ($Fe_{1-x}Si_x$, $x = 0.5$–1). For $x = 1$ (nominally pure Si interlayers) the coupling strength is exponentially decaying, and for $x = 0.5$ ($Fe_{0.5}Si_{0.5}$ interlayers) it exhibits an oscillating behavior and the overall coupling strength was reduced compared to the first case. Other groups also prepared epitaxial Fe/$Fe_{0.5}Si_{0.5}$/Fe sandwiches or multilayers which showed an exponential decrease of the EC with increasing $Fe_{0.5}Si_{0.5}$ thickness [17–20], in contrast to [16] and [21]. Usually these discrepancies are ascribed to deviations in the stoichiometry of the interlayer and the smoothness of the interfaces which were claimed to be very good in [16, 21]. It is interesting to note how small deviations in the stoichiometry of the interlayers from the $Fe_{0.5}Si_{0.5}$ composition can have drastic effects on the nature of the EC. For example, Croonenborghs *et al* [17] worked with a nominal composition of $Fe_{0.5}Si_{0.5}$ for the interlayer, whereas Gareev *et al* [21] applied a composition of $Fe_{0.56}Si_{0.44}$. In the first case an exponential decay of the coupling strength with increasing FeSi thickness was observed, and in the second case an oscillating behavior. Because the strongest AF coupling was always observed for nominally pure Si layers Gareev *et al* [1] rejected the original idea that metallic iron silicides at the interfaces are responsible for the strong EC in Fe/Si/Fe layers. For nominally pure Si the EC should be short ranged and exponentially decaying (according to the quantum interference model). Gareev *et al* [22, 23] indeed achieved a record EC of $>8$ mJ m$^{-2}$ by inserting a c-FeSi boundary layer at the bottom of Fe/Si/Fe structures. Furthermore, the AF coupling maximum was shifted to smaller Si thicknesses. The reason for these two results was attributed to reduced interdiffusion and the prevention of pinholes by the boundary layer, but direct experimental proof, at least for the diffusion, was unavailable at this time although the growth of all layers was shown to be epitaxial by LEED. Most interestingly the position of the coupling maximum was not shifted while varying the thickness of the bottom FeSi layer, and the onset of FM coupling was also not changed [23].

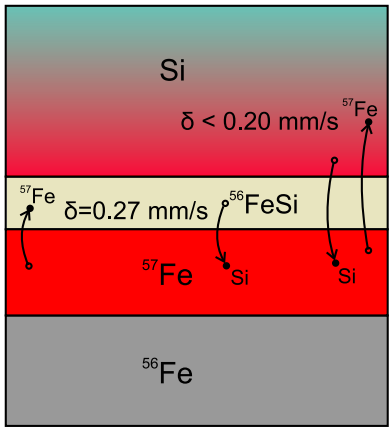


**Figure 1.** Illustration of the diffusion process at the Fe/FeSi/Si interfaces. The $^{57}$Fe probe atoms experience different isomer shifts $\delta$ depending on the Si content of their environment.

The goal of the present work is to shed light on the effectiveness of FeSi diffusion barriers in Fe/FeSi/Si multilayers and to find the effective FeSi thickness at which Fe diffusion into the Si layer is completely inhibited. Furthermore we want to study at which FeSi layer thickness the metastable c-FeSi phase forms and if additional silicide phases are observed. Additionally, the correlation of the exchange coupling with FeSi thickness is examined with ferromagnetic resonance (FMR) and superconducting quantum interference device magnetometry (SQUID). We conducted a systematic study on Fe/$Fe_{0.5}Si_{0.5}$/Si/$Fe_{0.5}Si_{0.5}$/Fe multilayers grown on Si(111) by molecular beam epitaxy (MBE). The nominal $Fe_{0.5}Si_{0.5}$ layer thickness was varied from 0 to 14 Å. $^{57}$Fe conversion electron Mössbauer spectroscopy (CEMS) in combination with the tracer layer technique [24–28] was applied at RT in order to investigate the diffusion of Fe and Si at the Fe/$Fe_{0.5}Si_{0.5}$/Si boundaries, which is illustrated in figure 1. Due to the isotope-selective detection of the conversion electrons the atomistic information about magnetism and structure in layers and at interfaces can be obtained with a high depth selectivity (typically a few atomic layers) using $^{57}$Fe enriched thin layers. The various Fe–Si phases can be well distinguished by Mössbauer spectroscopy because they differ in their hyperfine interactions. The most important Mössbauer hyperfine-interaction parameters are the isomer shift $\delta$, the quadrupole splitting $\Delta E_Q$ (observable in non-magnetic materials) and the magnetic Zeeman splitting caused by the hyperfine magnetic field, $B_{hf}$, at the $^{57}$Fe nucleus [29]. $\delta$ depends on the total s-electron density at the $^{57}$Fe nuclei in the sample, $\Delta E_Q$ is a measure of the deviation from local cubic symmetry around the $^{57}$Fe atom that leads to an electric field gradient (EFG), and $B_{hf}$ originates from the total electron spin density at the $^{57}$Fe nucleus and is observable in magnetically ordered phases or in materials with slow electronic Fe-3d spin

relaxation. Complementary results were obtained from x-ray diffraction (XRD), reflection high-energy electron diffraction (RHEED), SQUID magnetometry and FMR.

## 2. Experimental details

All samples were grown in ultrahigh vacuum (UHV) by MBE under the same conditions. The base pressure was $1 \times 10^{-10}$ mbar. For each sample the relevant periods of the multilayers were repeated five times. Therefore each sample contains four pairs of iron layers which are separated by the interlayers. Prior to the deposition the Si(111) substrates were rinsed in acetone, ethanol and 20% HF acid and then loaded into the UHV system. Finally they were heated to 900 °C in UHV to remove the silicon oxide. In order to minimize Si diffusion from the Si substrate and achieve initial epitaxial growth, the first step in the preparation was the evaporation of 10 Å thick $FeSi_2$ buffer layers which were carefully annealed for 15 min at 420 °C in order to promote the formation of the $\gamma$-$FeSi_2$ phase [30]. All samples were capped with 20 Å Cr for protection. Three types of samples were prepared which differ in the way the $^{57}$Fe tracer layer was incorporated (see figure 2).

Samples of type A contain a 6 Å thick $^{57}$Fe tracer layer directly below the $^{56}$FeSi boundary layer of thickness $t_{FeSi}$, which was varied between 0 and 14 Å. Samples of type B contain a 6 Å thick $^{56}$Fe layer separating the Si layer and the $^{57}$Fe tracer layer. In samples of type C, the $^{57}$FeSi boundary layer itself is enriched with $^{57}$Fe. The Si and Fe thicknesses ($^{56}$Fe + $^{57}$Fe) were kept constant at 20 Å and 21 Å, respectively, for all samples, except for samples of type B. Samples of type A were used to study the diffusion of $^{57}$Fe into the a-Si layer. Samples of type B were investigated to study the diffusion of Si into the $^{57}$Fe layer and, finally, samples of type C were analyzed to study the phase formation in the $^{57}$FeSi layer. Nominally, the substrate temperature during deposition was kept near room temperature (∼50 °C). The deposition rates for Fe were 0.05 Å s$^{-1}$, and for Si 0.085 Å s$^{-1}$, for both the pure layers and the boundary layers. The FeSi layers were prepared as artificial multilayers (digital alloys) with an effective FeSi rate of 0.133 Å s$^{-1}$. $^{57}$Fe, $^{56}$Fe and Cr were evaporated from resistively heated evaporation cells, while Si was evaporated from an electron gun. The depleted $^{56}$Fe metal contained a residual isotopic composition of 0.2% $^{57}$Fe and had a purity of 99.94 at.%. $^{57}$Fe was isotopically enriched to 95.5% and had a purity of 99.95 at.%. The film thicknesses and rates were measured with independent calibrated quartz crystal oscillators. The relative errors of the Fe, FeSi and Si thicknesses are 4%. For the alloy, in order to obtain the real FeSi thickness from the nominal (Fe + Si) thickness $t_{FeSi}$ measured by the quartz crystal oscillators, one has to apply a factor of 0.7 to the nominal thickness obtained from the quartz crystals, taking proper account of the different mass densities of Fe, Si and FeSi. The FeSi thickness $t_{FeSi}$ given here is the nominal thickness, if not stated otherwise. Additionally, the film growth was monitored by RHEED with an $e^-$-beam energy of 15 kV and a current of 30 $\mu$A. For CEMS at RT, a $^{57}$Co source embedded in an Rh matrix was used. The samples were mounted in a gas-flow proportional counter which used a He-5% $CH_4$ mixture.

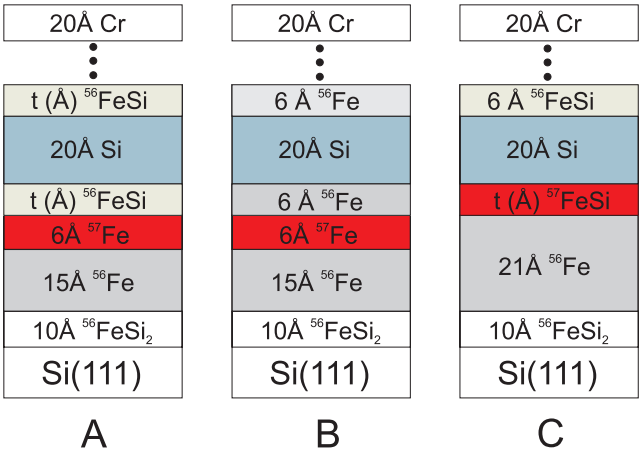


**Figure 2.** The geometrical structure of the prepared samples of type A, B and C.

The CEM spectra, all measured in zero external field, were least-squares fitted with the computer program NORMOS [31]. All isomer shifts are given relative to $\alpha$-Fe at RT. $\theta$–$2\theta$ high-angle and low-angle x-ray diffraction (XRD) were performed with Cu K$\alpha$ radiation. The magnetometry measurements were carried out in a commercial SQUID magnetometer (Quantum Design MPMS). FMR was conducted at RT with a microwave frequency of $f_0 = 9.8$ GHz, and with the magnetic field applied in the sample plane. The field was continuously varied from 0.0 to about 0.2 T.

## 3. Results and discussion

### *3.1. Structural analysis*

High-angle XRD measurements were performed to determine the layer structure and its epitaxial relationship. All $\theta$–$2\theta$ scans of our samples (not shown) exhibit a weak broadened reflection at $2\theta \approx 45°$, which was assigned to Fe(110) with slightly reduced lattice constants. Using thicker FeSi layers the lattice constant deduced from the Fe(110) reflection approaches the value of pure iron of 2.87 Å. The same effect was observed by increasing the Fe thickness itself, which leads to the main conclusion that an increasing FeSi thickness reduces the diffusion of Fe into the Si layer. This is supported by the CEMS measurements (see below). Figure 3 shows typical low-angle x-ray reflectivity data of samples of type A ($t_{FeSi} = 10$ Å) and type B ($t_{FeSi} = 0$ Å). All reflectivity curves exhibit superstructure Bragg reflections from the multilayer periodicity and fast oscillating Kiessig fringes due to the total thickness interference. Both observations indicate that our samples have a good multilayer periodicity and flat surfaces. The enhancement of the oscillations for $t_{FeSi} = 10$ Å indicates that by inserting FeSi layers the interface quality is improving.

RHEED measurements during deposition of the multilayers gave interesting insights into the growth mode and the morphology of our samples. Epitaxial island growth was found for the very first Fe and FeSi layers (figures 4(a) and (b)). The following Si formed an amorphous layer (not shown). The second FeSi layer also grew in its

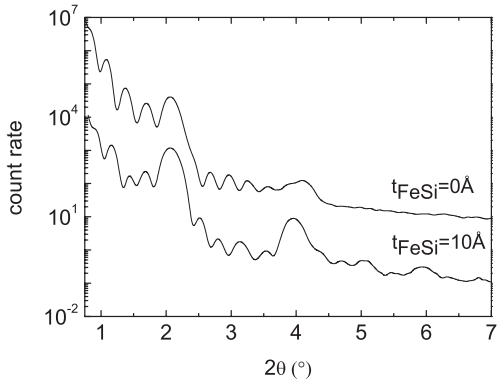


**Figure 3.** Typical low-angle x-ray reflectivity of sample type A with a nominal FeSi thickness of $t_{\mathrm{FeSi}} = 10$ Å (lower curve) and sample type B with $t_{\mathrm{FeSi}} = 0$ Å (upper curve).

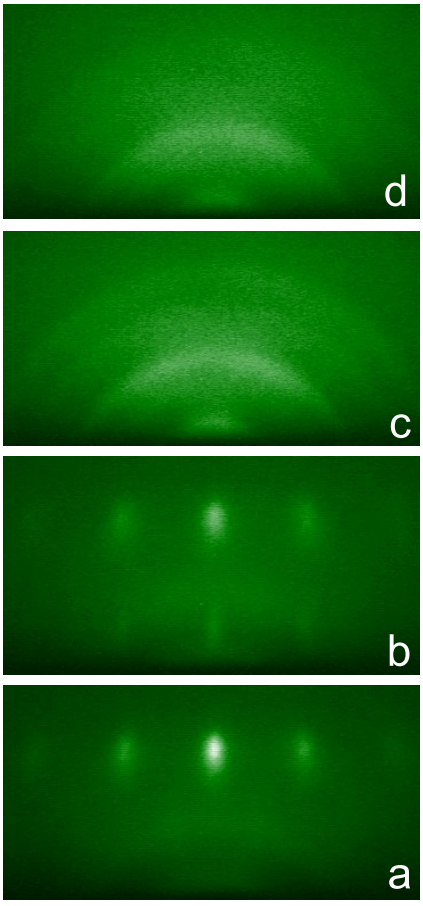


**Figure 4.** RHEED patterns of the first sample layers (images of the buffer layer and the amorphous Si and FeSi layers have been omitted). (a) 15 Å $^{56}$Fe, (b) 22 Å FeSi, (c) 9 Å Fe, (d) 10 Å FeSi.

amorphous state (not shown). Interestingly, the following second Fe and third FeSi layers grew in polycrystalline states, which was concluded from the observation of Debye–Scherrer rings (figures 4(c) and (d)).

These results demonstrate that the FeSi/Si and Si/FeSi interfaces are inequivalent, which was also observed in [10]. Due to the epitaxial growth for the first Fe and FeSi layer

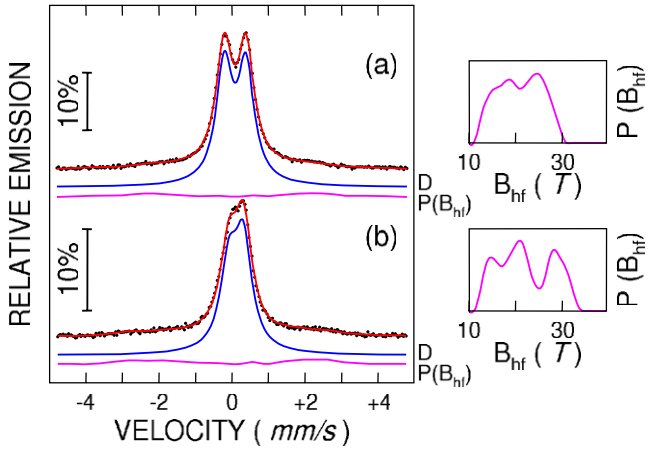


**Figure 5.** Typical CEM spectra of sample type C with $t_{\mathrm{FeSi}} = 6$ Å (a) and $t_{\mathrm{FeSi}} = 20$ Å (b). The spectra were fitted with two subspectra: a dominant quadrupole doublet D and a weak magnetic hyperfine field distribution $P(B_{\mathrm{hf}})$ (right-hand side).

it was possible to extract information about the relaxation of their respective in-plane lattice parameters. For this purpose we used the Bragg formula $d_{\mathrm{f}} = (k_{\mathrm{s}}/k_{\mathrm{f}})d_{\mathrm{s}}$, with $d_{\mathrm{f}}$ and $d_{\mathrm{s}}$ being the in-plane atomic distances for film and substrate, respectively, and $k_{\mathrm{f}}$ and $k_{\mathrm{s}}$ the positions in $k$ space of the first-order diffraction spots relative to the zero-order reflection for film and substrate, respectively. For Fe, the relaxation process was found to end at a thickness of approx. 10 Å, starting from a value of 2.73 Å of $\gamma$-FeSi$_2$. In contrast, the relaxation of the FeSi film is only finished up to 18 Å, with a final value of the lattice constant of 2.77 Å, matching closely the value of c-FeSi [32, 33].

### *3.2. Mössbauer spectroscopy*

To investigate the structural phase of the FeSi diffusion barriers we analyze CEM spectra of sample type C ($^{57}$FeSi tracer layers), as shown in figure 5. They were fitted with a dominant quadrupole doublet D and a weak subspectrum with a magnetic hyperfine distribution $P(B_{\mathrm{hf}})$. For a thickness of $t_{\mathrm{FeSi}} = 6$ Å (figure 5(a)) the values for the isomer shift $\delta$ and the quadrupole splitting $\Delta E_{\mathrm{Q}}$ of the doublet are $\delta = 0.20(1)$ mm s$^{-1}$ and $\Delta E_{\mathrm{Q}} = 0.60(1)$ mm s$^{-1}$. A doublet with virtually identical hyperfine parameters was also detected in Fe/Si multilayers [3] and Fe/Fe$_x$Si$_{1-x}$ multilayers [2]. However, for $t_{\mathrm{FeSi}} = 20$ Å (figure 5(b)) one obtains values of $\delta = 0.22(1)$ mm s$^{-1}$ and $\Delta E_{\mathrm{Q}} = 0.39(2)$ mm s$^{-1}$.

In figures 5(a) and (b) the area (relative intensity) of the subspectrum with the distribution $P(B_{\mathrm{hf}})$ amounts to only 10% and 18%, respectively, of the total spectral area, providing only a weak contribution. The spectral parameters of the c-FeSi phase are $\delta = 0.26$ mm s$^{-1}$ and $\Delta E_{\mathrm{Q}} = 0.15(1)$ mm s$^{-1}$, according to the literature [18, 33–37]. This metastable phase crystallizes in the B2 (or CsCl) structure with space group $Pm\bar{3}m$ [33]. This is a bcc lattice with Si at the origin and Fe at $(1/2, 1/2, 1/2)$. Fe and Si are both coordinated with eight nearest neighbors of different kinds. The corresponding bulk stable phase is $\epsilon$-FeSi which is also cubic but has the

space group $P2_13$ ($T^4$) [33]. In the ideally cubic c-FeSi phase no quadrupole splitting should be observed. One attempt to explain our large $\Delta E_Q$ value for $t_{FeSi} = 6$ Å (figure 5(a)) is the lattice deformation of the film [35], which produces an electric field gradient, since for this small thickness the lattice relaxation is still not yet finished, as confirmed by our RHEED results. There exists a linear correlation [35] between lattice mismatch and quadrupole splitting for c-FeSi films thinner or equal to 50 Å of $\frac{(-18.6\%)}{(\text{mm s}^{-1})}$. However, taking into account our quadrupole splitting of $\Delta E_Q = 0.60(1)$ mm s$^{-1}$ one obtains an unreasonable mismatch of $-11.2\%$, which is in contrast to the maximum attainable mismatch between c-FeSi and Fe of $-3.5\%$. A more reasonable explanation for our results is the formation of a defective c-$Fe_{0.5}Si$ phase for thin FeSi layers. It contains defects which consist of $n = 0$–6 vacancies as next-nearest neighbors of a central $^{57}$Fe atom [37]. The parameters for $n = 3$ ($\delta = 0.24(1)$ mm s$^{-1}$ and $\Delta E_Q = 0.54(1)$ mm s$^{-1}$) are similar to ours for $t_{FeSi} = 6$ Å. The strong decrease of $\Delta E_Q$ for thicker FeSi films (figure 5(b)) and the increase of $\delta$ can be attributed to better ordering and better homogeneity of the crystal structure, which leads to a less disturbed c-FeSi phase. The origin of the magnetic distribution $P(B_{hf})$ in figure 5 can be twofold. A small excess of Fe during evaporation can lead to non-stoichiometric regions in the FeSi layer which behave ferromagnetically. Walterfang *et al* [36] observed average magnetic hyperfine fields $\langle B_{hf}\rangle$ with values smaller than 3 T at RT for Fe excess of 4.5 at.% in thin c-FeSi films on MgO. This was attributed to the presence of a fraction of a non-stoichiometric c-$Fe_xSi_{1-x}$ phase in the FeSi film. We observe much higher $\langle B_{hf}\rangle$ values ($\langle B_{hf}\rangle = 20.9$ T and 22.6 T for $t_{FeSi} = 6$ Å and 20 Å, respectively) which, in turn, would suggest a much higher Fe excess during evaporation than 4.5%, since $\langle B_{hf}\rangle$ scales with the Si content. Due to the use of calibrated quartz monitors this situation is unlikely. It is more probable that mixing at the $^{56}$Fe/$^{57}$FeSi interface leads to the formation of a ferromagnetic solution or phase similar to $Fe_3Si$ during Fe evaporation on Si, if one exceeds a certain Fe thickness, as described in section 1.

To elucidate the functionality of the FeSi diffusion barrier we now analyze CEM spectra of sample types A and B ($^{57}$Fe tracer layers), as shown in figure 6. The spectra of sample type A (figures 6(a)–(c)) were fitted with two subspectra: a quadrupole doublet D1 and a magnetic hyperfine field distribution $P(B_{hf})$.

The magnetic distributions $P(B_{hf})$ originate from the $^{57}$Fe atoms at the $^{57}$Fe/$^{56}$FeSi interface which experiences an Fe-rich environment and therefore a magnetic hyperfine field. The spectral areas of the doublet D1 are the sum of two contributions. The first one originates from $^{57}$Fe atoms which diffused into the $^{56}$FeSi layer. The second one is due to $^{57}$Fe atoms which diffused through the $^{56}$FeSi layer into the a-Si layer. One observes that, for increasing FeSi thickness $t_{FeSi}$, the relative spectral area of the doublet D1 experiences a strong decrease: starting from 39% for $t_{FeSi} = 0$ Å and decreasing to 21% for $t_{FeSi} = 3$ Å, it finally reaches 3% for $t_{FeSi} = 14$ Å (figures 6(a)–(c)). The interpretation of this result is that, for the thicker and less defective FeSi layers (14 Å), the diffusion of $^{57}$Fe is inhibited, but even for relatively

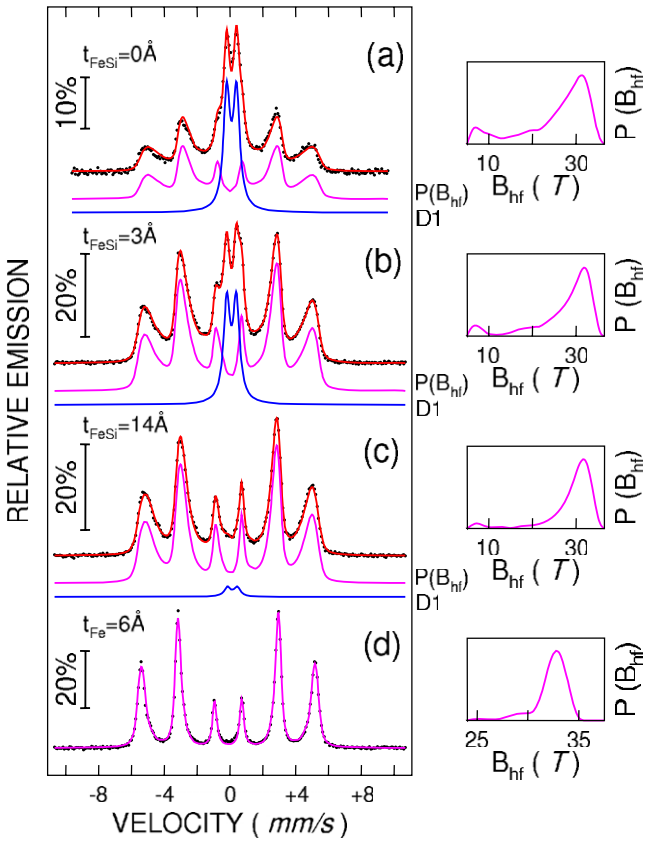


**Figure 6.** Typical CEM spectra of sample types A and B. The nominal FeSi thickness for sample type A was $t_{FeSi} = 0$ Å (a), 3 Å (b) and 14 Å (c). The $^{56}$Fe thickness for sample type B was $t_{Fe} = 6$ Å (d). Spectra of type A were fitted with two subspectra: a quadrupole doublet D1 and a magnetic hyperfine field distribution $P(B_{hf})$. The spectrum of type B was fitted with a magnetic hf field distribution $P(B_{hf})$ only (right-hand side).

thin layers (3 Å) which contain a higher amount of defects, the diffusion is strongly suppressed. For the CEM spectrum of sample type B (figure 6(d)) with a 6 Å $^{56}$Fe layer instead of $^{56}$FeSi it was sufficient for the fitting to use a relatively sharp magnetic distribution $P(B_{hf})$. The maximum of the distribution is located at $B_{hf} = 33$ T, which is identical to the value of pure $\alpha$-Fe. The sharpness of the distribution and the absence of a doublet shows that the diffusion of Si into the $^{57}$Fe probe layer is negligible and the main diffusing species at RT is Fe, as was also shown in [10]. CEMS measurements on amorphous $Fe_{1-x}Si_x$ layers [38–41] and $^{57}$Fe ion-implanted silicon [42] showed a correlation between isomer shift $\delta$ and Si concentration $x$, as exhibited in figure 7. With decreasing $x$, starting from high Si content, the isomer shift first drops from $\sim$0.2 to $\sim$0.13 mm s$^{-1}$ and then increases again until it reaches the highest value of $\sim$0.28 mm s$^{-1}$ for crystalline $\epsilon$-FeSi [33] which corresponds to a Si content of $x = 0.5$.

Our results for the evolution of the isomer shift $\delta$ and the relative spectral area (inset) of doublet D1 with increasing $t_{FeSi}$ are shown in figure 8. Starting from $t_{FeSi} = 0$ Å, $\delta$ drops slightly from 0.23 to 0.21 mm s$^{-1}$ and then again increases to 0.235 mm s$^{-1}$ at $t_{FeSi} = 10$ Å. A further increase of $t_{FeSi}$ is accompanied by a jump (vertical dotted line) of $\delta$ to

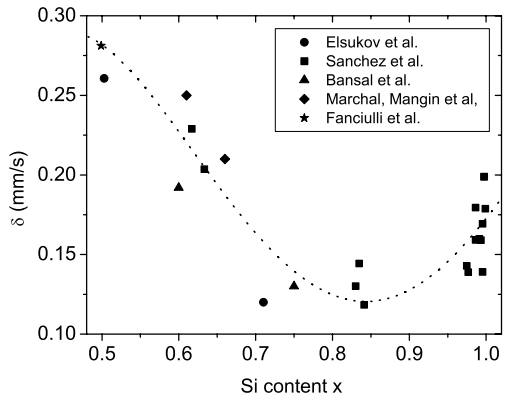


**Figure 7.** Correlation between isomer shift $\delta$ and silicon content $x$ in $Fe_{1-x}Si_x$ alloys. The dashed line is a guide for the eyes.

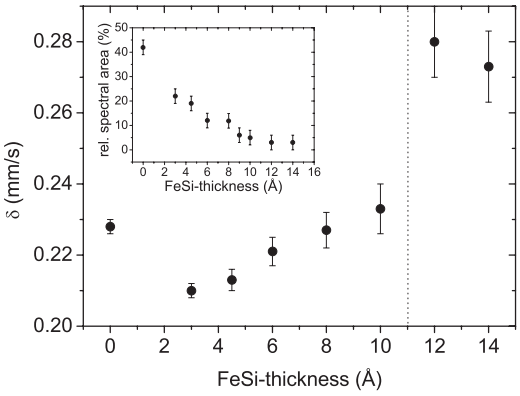


**Figure 8.** Isomer shift $\delta$ of the doublet D1 (sample type A) versus nominal FeSi thickness $t_{FeSi}$. The inset displays the evolution of the relative spectral area of the doublet D1 with increasing FeSi thickness $t_{FeSi}$.

0.27–0.28 mm $s^{-1}$. Simultaneously, the relative spectral area of D1 decreases monotonically from initially 42% down to 3% for $t_{FeSi} = 14$ Å (inset, figure 8). The interpretation of these results is as follows. For the region $t_{FeSi} = 0$–10 Å we have a superposition of quadrupole doublets with isomer shifts of less than 0.20 mm $s^{-1}$, originating from $^{57}$Fe atoms in the a-Si layer (Si-rich environment) and of $\delta = 0.27$ mm $s^{-1}$ from the $^{56}$FeSi layer, leading to an overall isomer shift $\delta \leqslant 0.23$ mm $s^{-1}$. Increasing $t_{FeSi}$ further inhibits the diffusion of $^{57}$Fe atoms through the FeSi layer into the a-Si. This leads to an increase of the overall $\delta$ of D1. One can compare this progress of $\delta$ directly with figure 7 but has to keep in mind that we are starting from high Si content, which is located at the right-hand side of figure 7, and move to the left for increasing $t_{FeSi}$ (lower Si content). The jump of $\delta$ for $t_{FeSi} \approx 11$ Å to ~0.27 mm $s^{-1}$ corresponds to a sudden change of the Si content in the environment of the $^{57}$Fe probe atoms to $x = 0.5$. This marks the critical thickness $t_{FeSi}$ at which no $^{57}$Fe diffuses into the a-Si layer. Since the area of D1 for these thicknesses becomes very small (see inset figure 8) this also means that only a negligible amount of $^{57}$Fe diffuses into the $^{56}$FeSi layer itself. The remaining magnetic distribution $P(B_{hf})$ corresponds to slightly disturbed $\alpha$-Fe and a very small

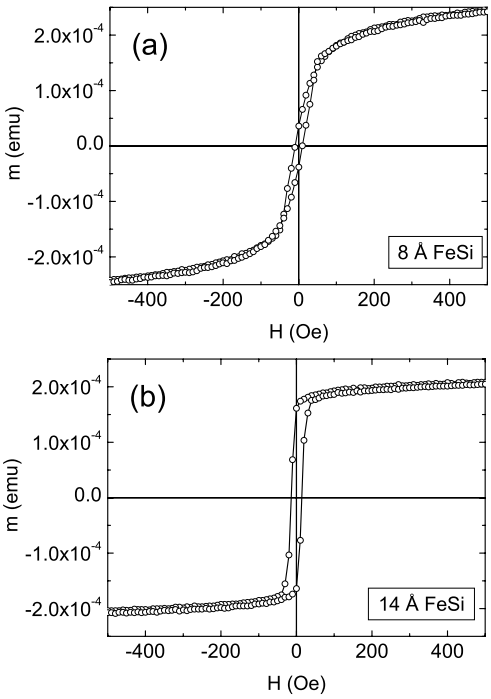


**Figure 9.** Typical hysteresis loops (sample type A) at RT for $t_{FeSi} = 8$ Å (a) and $t_{FeSi} = 14$ Å (b).

contribution of FeSi alloys with a nominal composition of $Fe_{55}Si_{45}$ to $Fe_{65}Si_{35}$. These estimations are extracted from the evolution of the hyperfine field distributions $P(B_{hf})$ with $t_{FeSi}$ (see [36]).

### *3.3. SQUID magnetometry and FMR*

In order to examine the strength and the sign of the exchange coupling as a function of $t_{FeSi}$ in our structures we performed SQUID and FMR measurements. Typical hysteresis loops are shown in figure 9. The first loop (figure 9(a)) for $t_{FeSi} = 8$ Å has a low remanence and large saturation field, typical for AF coupled systems. By contrast, for $t_{FeSi} = 14$ Å the remanence of the hysteresis loop is higher and the sample saturates at lower fields. This already hints at some kind of oscillations in the exchange coupling strength. From the analysis of the hysteresis loops at RT we obtained the parameter $F_{AF} = 1 - M_R/M_S$. $M_R$ refers to the remanent magnetization and $M_S$ to the saturation magnetization ($M_S$ was taken at an external field of 2 T for all samples). The common assumption is that this parameter is proportional to the amount of AF coupled regions of the sample [43]. If $F_{AF} = 1$ the whole sample is AF coupled, while if $F_{AF} = 0$ the coupling is FM.

Care has to be taken if one extracts the strength of the AF coupling from this parameter. However, as already pointed out by den Broeder *et al* [44], this parameter is rather a measure of an incomplete AF alignment which can be frequently caused by pinholes, the latter causing FM coupling. A direct confirmation of the sign of the EC can be assessed by FMR. Due to the coupling of the Fe films across the interlayers one observes an acoustical mode and an optical mode in the precession of the Fe films. Since the dispersion relations are

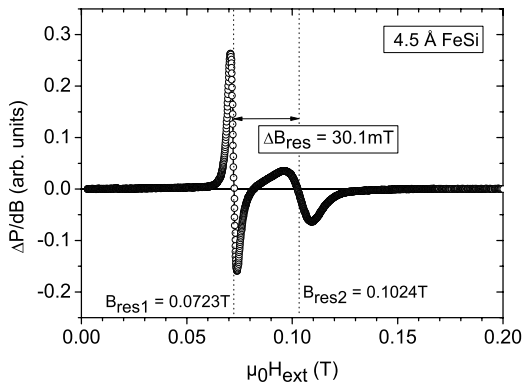


**Figure 10.** FMR spectrum of sample type A ($t_{\mathrm{FeSi}} = 4.5$ Å) with two resonance fields at $B_{\mathrm{res1}}$ and $B_{\mathrm{res2}}$ ($f_0 = 9.8$ GHz).

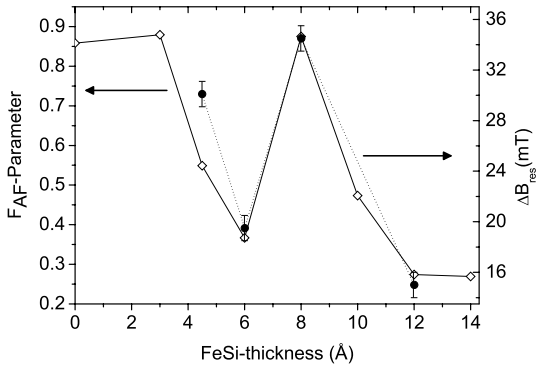


**Figure 11.** $F_{\mathrm{AF}}$ parameter (open diamonds) and splitting of the resonance fields $\Delta B_{\mathrm{res}}$ (full circles) from SQUID hysteresis loops and FMR measurements, respectively, versus nominal FeSi thickness $t_{\mathrm{FeSi}}$.

different for FM or AF coupling, a distinction between these two can be made by looking at the relative positions of the absorption lines, taking into account that the optical mode has always less intensity than the acoustical mode [45, 46]. The splitting of the two modes $\Delta B_{\mathrm{res}}$ provides the strength of the coupling. A typical FMR spectrum is shown in figure 10. Since the external field is modulated at a frequency of 100 kHz in order to enhance the sensitivity of the measurement with the lock-in technique, one observes differentiated Lorentzian absorption lines.

The absorption spectrum in figure 10 was fitted with a sum of two differentiated Lorentzian lines. The resonance fields are found from the zero crossings of the fit ($B_{\mathrm{res1}}$ and $B_{\mathrm{res2}}$, see figure 10). One observes that the optical mode appears at higher external fields, which conclusively means that the Fe films are AF coupled in this sample [45, 46]. In fact, AF coupling was observed in all of our samples. The strength of the coupling can be calculated via the formula $\Delta B_{\mathrm{res}} = J_{\mathrm{EC}}/M_{\mathrm{s}}d$ for symmetric interlayer-coupled multilayers [46], with $\Delta B_{\mathrm{res}}$, $J_{\mathrm{EC}}$, $M_{\mathrm{s}}$ and $d$ being the effective exchange field (splitting of the acoustical and optical mode), the exchange coupling constant, the saturation magnetization and the thickness of one Fe layer, respectively. However, our RHEED measurements (section 3.1) prove that we are dealing with an asymmetric multilayer system here, where the FeSi/Si and Si/FeSi interfaces are found to be inequivalent. As stated explicitly in [46], in the latter case the exchange coupling $J_{\mathrm{EC}}$ is not determined any more by the simple equation for $\Delta B_{\mathrm{res}}$ given above. Therefore we refrain from calculating $J_{\mathrm{EC}}$ from our measured $\Delta B_{\mathrm{res}}$ values. We like to emphasize, however, that the measured $\Delta B_{\mathrm{res}}$ values provide a measure of the relative coupling strength. The combined results of SQUID and FMR measurements are shown in figure 11. It is remarkable that both parameters correlate very well with each other, which was not expected beforehand, most notably for $F_{\mathrm{AF}}$, as discussed before. One observes a clear oscillation of the coupling strength with maxima at $t_{\mathrm{FeSi}} = 3.5$ Å and $t_{\mathrm{FeSi}} = 8$ Å. There is a small damping of the oscillation, since the $F_{\mathrm{AF}}$ value at $t_{\mathrm{FeSi}} = 12$ Å is clearly lower than the value at the minimum at $t_{\mathrm{FeSi}} = 6$ Å. Since our main investigation was focused on the diffusion of Fe, which was suppressed for thicknesses starting from 12 Å, we did not investigate samples with higher FeSi thicknesses than 14 Å. The observed AF-type oscillation is in qualitative accordance with theoretical predictions by Herper *et al* [47].

It has to be mentioned that in [47], although inhomogeneous alloy formation at the interfaces of Fe/Si/Fe trilayers was taken into account, the Si lattice was simulated within a bcc structure with a lattice constant of 5.27 Å. This in turn produced a metallic Si lattice. Comparing our results in figure 11 more closely with similar behavior observed by Bürgler *et al* [16] for pure FeSi interlayers without Si, one observes subtle differences. The two maxima in [16] were observed at $t_{\mathrm{FeSi}} = 18$ and 39 Å. We can conclude that our first maximum is extended to a higher total thickness $t_{\mathrm{S}}$ of 26 Å ($t_{\mathrm{S}} = 2t_{\mathrm{FeSi}} + t_{\mathrm{Si}}$) than in [16]. However, our second maximum at $t_{\mathrm{S}} = 2 \times 8$ Å $+ 20$ Å $= 36$ Å is only slightly shifted in comparison to that in [16]. A tentative interpretation of this result could be that the interfacial disorder in our samples with the thinnest FeSi boundary layers produces a phase shift and/or an amplitude change of the oscillating exchange coupling. The physical origin is an additional cosine-like term in the exchange coupling from the specular reflection of the electron waves at the disordered interfaces [48]. For thicker FeSi layers this effect is negligible since the disorder is strongly reduced due to the formation of the non-defective c-FeSi phase.

## 4. Conclusions

We have successfully studied the interdiffusion processes in Fe/FeSi/Si/FeSi/Fe multilayers on Si(111) via CEMS. We demonstrate that the insertion of FeSi boundary layers suppresses the Fe/Si interdiffusion leading to better defined interfaces. A complete prevention of the Fe diffusion was found for $t_{\mathrm{FeSi}} = 10$–12 Å. This result allows for a reliable investigation of interlayer exchange coupling at this or greater FeSi thicknesses. The evolution of the slightly defective c-FeSi phase for thicker FeSi films was confirmed by RHEED and CEMS. All our samples exhibit oscillating antiferromagnetic interlayer coupling, as confirmed by FMR. The oscillation period of this coupling is approx. 6 Å, which was also observed by SQUID. Our finding is in qualitative agreement

with theoretical predictions by Herper *et al* [47]. Future work will include the investigation of the coupling for variable Si thickness, since in the present work the main focus was on the FeSi boundary layer.

## Acknowledgments

We are indebted to U v Hörsten for his valuable technical assistance. Fruitful discussions with M Walterfang and R A Brand are highly appreciated. This work was supported by the Deutsche Forschungsgemeinschaft (in part by grant nos. Ke 273/18-2 and SFB 491).

## References

[1] Gareev R R, Bürgler D E, Buchmeier M, Schreiber R and Grünberg P 2002 *J. Magn. Magn. Mater.* **240** 235
[2] Kopcewicz M, Luciński T and Wandziuk P 2005 *J. Magn. Magn. Mater.* **286** 488
[3] Luciński T, Kopcewicz M, Hütten A, Brückl H, Heitmann S, Hempel T and Reiss G 2003 *J. Appl. Phys.* **93** 6501
[4] Luciński T, Wandziuk P, Stobiecki F, Andrzejewski B, Kopcewicz M, Hütten A, Reiss G and Szuszkiewicz W 2004 *J. Magn. Magn. Mater.* **282** 248
[5] Fanciulli M, Degroote S, Weyer G and Langouche G 1997 *Surf. Sci.* **377** 529
[6] Fanciulli M, Zenkevich A and Weyer G 1998 *Appl. Surf. Sci.* **123** 207
[7] Dézsi I, Fetzer C, Szücks I, Dekoster J, Vantomme A and Caymax M 2005 *Surf. Sci.* **599** 122
[8] Alvarez J, de Parga A L V, Hinarejos J J, de la Figuera J, Michel E G, Ocal C and Miranda R 1993 *Phys. Rev.* B **47** 16048
[9] Kläsges R, Carbone C, Eberhardt W, Pampuch C, Rader O, Kachel T and Gudat W 1997 *Phys. Rev.* B **56** 10801
[10] Strijkers G J, Kohlhepp J T, Swagten H J M and de Jonge W J M 1999 *Phys. Rev.* B **60** 9583
[11] Moroni E G, Wolf W, Hafner J and Podloucky R 1999 *Phys. Rev.* B **59** 12860
[12] Imazono T, Hirayama Y, Ichikura S, Kitakami O, Yanagihara M and Watanabe M 2004 *Japan. J. Appl. Phys.* **43** 4327
[13] Endo Y, Kitakami O and Shimada Y 1997 *J. Magn. Soc. Japan.* **21** 541
[14] Bruno P 1995 *Phys. Rev.* B **52** 411
[15] Endo Y, Kitakami O and Shimada Y 1999 *Phys. Rev.* B **59** 4279
[16] Bürgler D E, Buchmeier M, Cramm S, Eisebitt S, Gareev R R, Grünberg P, Jia C L, Pohlmann L L, Schreiber R, Siegel M, Qin Y L and Zimina A 2003 *J. Phys.: Condens. Matter* **15** S443
[17] Croonenborghs B, Almeida F M, Gareev R R, Rots M, Vantomme A and Meersschaut J 2005 *Phys. Rev.* B **71** 024410
[18] Dekoster J, Degroote S, Meersschaut J, Moons R, Vantomme A, Bottyán L, Deák L, Szilágyi E, Nagy D L, Bacon A Q R and Langouche G 1999 *Hyperfine Interact.* **120/121** 39
[19] de Vries J J, Kohlhepp J, den Broeder F J A, Coehoorn R, Jungblut R, Reinders A and de Jonge W J M 1997 *Phys. Rev. Lett.* **78** 3023
[20] Fullerton E E, Mattson J E, Lee S R, Sowers C H, Huang Y Y, Felcher G and Bader S D 1992 *J. Magn. Magn. Mater.* **117** L301
[21] Gareev R R, Bürgler D E, Buchmeier M, Olligs D, Schreiber R and Grünberg P 2001 *Phys. Rev. Lett.* **87** 157202
[22] Gareev R R, Bürgler D E, Buchmeier M, Schreiber R and Grünberg P 2002 *Appl. Phys. Lett.* **81** 1264
[23] Gareev R R, Bürgler D E, Buchmeier M, Schreiber R and Grünberg P 2002 *Trans. Magn. Soc. Japan* **2** 205
[24] Sauer C and Zinn W 1993 *Magnetic Multilayers* ed L H Bennett and R E Watson (Singapore: World Scientific)
[25] Shinjo T and Keune W 1999 *J. Magn. Magn. Mater.* **200** 598
[26] Macedo W A A, Sahoo B, Kuncser V, Eisenmenger J, Felner I, Nogues J, Liu K, Keune W and Schuller I K 2004 *Phys. Rev.* B **70** 224414
[27] Stromberg F, Keune W, Kuncser V E and Westerholt K 2005 *Phys. Rev.* B **72** 064440
[28] Sahoo B, Macedo W A A, Keune W, Kuncser V E, Eisenmenger J, Nogues J, Schuller I K, Felner I, Liu K and Röhlsberger R 2006 *Hyperfine Interact.* **169** 1371
[29] Gonser U 1975 *Mössbauer Spectroscopy* ed U Gonser (Heidelberg: Springer)
[30] von Känel H, Stalder R, Sirringhaus H, Onda N and Henz J 1991 *Appl. Surf. Sci.* **53** 196
[31] Brand R A 1987 *Nucl. Instrum. Methods Phys. Res.* B **28** 398
[32] Al-Sharif A I, Abu-Jafar M and Qteish A 2001 *J. Phys.: Condens. Matter* **13** 2807
[33] Fanciulli M, Weyer G, Svane A, Christensen N E, von Känel H, Müller E, Onda N, Miglio L, Tavazza F and Celino M 1999 *Phys. Rev.* B **59** 3675
[34] Degroote S, Vantomme A, Dekoster J and Langouche G 1995 *Appl. Surf. Sci.* **91** 72
[35] Croonenborghs B, Almeida F M, Cottenier S, Rots M, Vantomme A and Meersschaut J 2004 *Appl. Phys. Lett.* **85** 200
[36] Walterfang M, Keune W, Trounov K, Peters R, Rücker U and Westerholt K 2006 *Phys. Rev.* B **73** 214423
[37] Fanciulli M, Rosenblad C, Weyer G, von Känel H and Onda N 1996 *Thin Solid Films* **275** 8
[38] Elsukov E P, Konygin G N, Barinov V A and Voronina E V 1992 *J. Phys.: Condens. Matter* **4** 7597
[39] Bansal C, Campbell S J and Stewart A M 1982 *J. Magn. Magn. Mater.* **27** 195
[40] Mangin P and Marchal G 1978 *J. Appl. Phys.* **49** 1709
[41] Marchal G, Mangin P, Piecuch M and Janot C 1976 *J. Physique Coll.* **37** 763
[42] Sánchez F H, van Raap M B F and Desimoni J 1990 *Phys. Rev.* B **44** 4290
[43] Inomata K, Yusu K and Saito Y 1995 *Phys. Rev. Lett.* **74** 1863
[44] den Broeder F J A and Kohlhepp J 1995 *Phys. Rev. Lett.* **75** 3026
[45] Zhang Z, Zhou L, Wigen P E and Ounadjela K 1994 *Phys. Rev.* B **50** 6094
[46] Lindner J, Kollonitsch Z, Kosubek E, Farle M and Baberschke K 2001 *Phys. Rev.* B **63** 094413
[47] Herper H C, Weinberger P, Szunyogh L and Sommers C 2002 *Phys. Rev.* B **66** 064426
[48] Los V F and Los A V 2008 *Phys. Rev.* B **77** 024410